International Conference on Concentrating Solar Power and Chemical Energy Systems, SolarPACES 2014

3-D CFD modeling of a slanted receiver in a compact linear Fresnel plant with etendue-matched mirror field

A.E. Rungasamy[a], K.J. Craig[b]*, J.P. Meyer[c]

[a]Graduate student [b]PrEng, PhD, Professor [c]PrEng, PhD, Professor, Head of Department
Department of Mechanical and Aeronautical Engineering, University of Pretoria, Pretoria 0002, South Africa

Abstract

Compact linear Fresnel receivers can be modified to include an etendue conserving mirror field as opposed to a flat field. Etendue can be used as an indicator of the losses within the system and therefore the optical optimization of the mirror field seeks to conserve incoming etendue. This can be done once for peak conditions and subsequently fixed with mirrors rotating throughout the day; or the mirror axis points can also be allowed to move up and down throughout the day, creating new etendue conservation curves. Radiation is modeled using discrete ordinates with no conduction in a two-dimensional and the absorbed radiation flux profiles are subsequently patched onto a three-dimensional slanted receiver as a heat source. The commercial software package *ANSYS Fluent v15.0* was used together with the *Matlab* toolset to study the influence of different mirror fields on the amount of radiation transferred to the collector pipes.

Keywords: etendue matched mirror field; discrete ordinates radiation modeling; concentrated solar power; compact linear fresnel

1. Introduction

Linear Fresnel reflector (LFR) technology is a line focus model within the concentrated solar power field. While LFR technology is cheap and easy to maintain, it generally has lower associated efficiencies. However, new research suggests that the optical efficiency of LFR plants could become comparable to that of a parabolic trough.

---

* Corresponding author. Tel.: +27-12-420-3515.
  E-mail address: ken.craig@up.ac.za

Nomenclature

U_0	etendue of incoming radiation (m²sr)		H	height of the receivers (m)
U_1	etendue of reflected radiation to receiver 1 (m²sr)		D	width of the mirror field (m)
U_2	etendue of reflected radiation to receiver 2 (m²sr)		ξ_1,ξ_2	angle in radiation splitter (°)
α	angle of the curve (°)		γ_1,γ_2	angle in radiation splitter (°)
φ_1, φ_2	angle from point on the mirror to receiver 1,2 (°)		ϑ	sun angle(°)
x_p	x-coordinate for turning point of the parabola (m)			
y_p	y-coordinate for turning point of the parabola (m)			

LFR plants generally have lower efficiencies due to optical losses in the mirror field. These include blocking of reflected radiation and shading of mirrors from incoming radiation. A number of studies have sought to maximise the optical efficiency of the mirror field by adjusting the layout of the field [1], however few change both the position and the size of the mirrors. [2]

A compact linear Fresnel system creates multiple receiver targets for the reflectors, reducing optical losses as adjacent mirrors now have dissimilar angles [3]. This also reduces the amount of land required for a plant, thus making the implementation more cost effective. An etendue matched mirror field paired with a compact linear Fresnel layout and finite mirror sizes yielded a peak optical efficiency of approximately 85% [4]. Etendue is defined as the product of the solid angle subtended by the aperture's entrance and the area of the source and a system where the etendue of the incoming radiation is equal to the etendue of the outgoing radiation is an optical system with zero losses. An etendue matched mirror field therefore positions mirrors along a curve determined through etendue conservation and sizes mirrors based on the position within the field.

2. Mirror field calculations and problem formulation

In order to obtain the Etendue Conservation Curve the problem is formulated as a piecewise function with two parabolic sections at the start and end of the curve and a curve in the center which conserves etendue. Parabolic curves with a single target conserve etendue by definition, while Chaves [4] defines the etendue conservation for multiple targets which can be expressed as follows (with the symbols defined in Figure1)

$$dU_0 = 2dl \cos\alpha \sin\theta \qquad dU_0 = dU_1 + dU_2$$
$$dU_1 = 2dl \cos(\phi_1 - \alpha)\sin\theta \qquad 2dl\cos\alpha\sin\theta = 2dl\cos(\phi_1 - \alpha)\sin\theta + 2dl\cos(\phi_2 + \alpha)\sin\theta$$
$$dU_2 = 2dl\cos(\phi_2 + \alpha) \qquad \cos\alpha = \cos(\phi_1 - \alpha) + \cos(\phi_2 + \alpha)$$
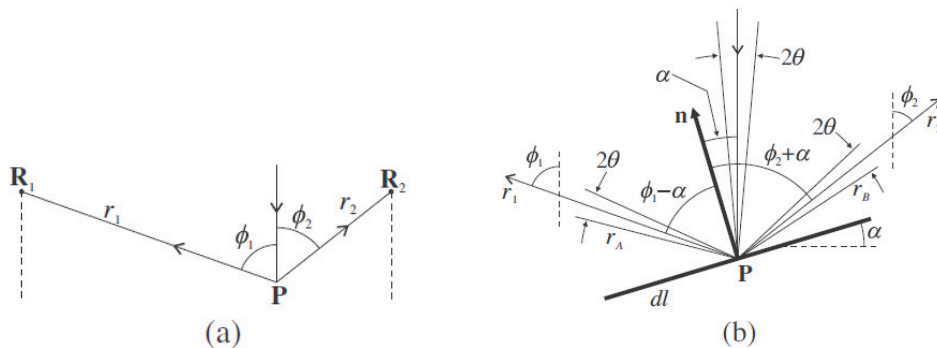

Figure 1. a) Schematic representation of the angles between the starting point P and the two receivers and b) Etendue balance diagram for light reflected to two receivers over length dl [4].

The mirror field is sized according to the receiver height (constant for all receivers), as the center of the field is at a distance that creates an angle of approximately 60° with the receivers due to the symmetry of the field and a fixed field aspect ratio. A receiver height (*H*) of 6.0m is chosen and the width of the mirror field established $D = 2H\tan 60$. The start points of the parabolas represent the limits of the mirror field domain and the end points of the parabola represent the transition point from a single target mirror field to a multiple target field. The governing equation for the parabolic sections is derived from the equation for the focal point of a parabola:

$$y(x) = \frac{(x - x_p)^2}{4y_f} + y_p$$

where the turning point of the first parabola is $(x_{p1}, y_{p1}) = (0,0)$ and the turning point of the second parabola is $(x_{p2}, y_{p2}) = (D, 0)$. The focal points of the parabolas y_f are the receiver heights (*H*) correlating to the section. Note that this transition point is significant, as multiple etendue conserving curves can be generated. The optimization is therefore dependent on its starting point and using the origin as the start point of the parabolas represents the most compact curve, thus reducing unnecessary structural material. The transition point represents the point at which the tangent to the curve passes through the opposite receiver. The tangent to the curve is defined as $\left(\dfrac{dy}{dx}\right)_{parabola} = \dfrac{2(x - x_p)}{4y_f}$, while the equation for the line through the receiver is defined as $\left(\dfrac{dy}{dx}\right)_{receiver} = \dfrac{H - y}{D - x}$. The point at which the two gradients are equal is found through a simpler optimization study which results in the end point of the parabola. This transition point represents the start of the unconstrained optimization study which seeks to minimise the following objective function

$$f(x) = \left|\left[\cos(\phi_1 - \alpha) + \cos(\phi_2 + \alpha)\right] - \cos\alpha\right|$$

The resultant curve then needs to be discretized from a continuous surface to individual mirrors. The peak curve is symmetric about the center of the field and the turning point lies at y = 0 (See Figure 2).
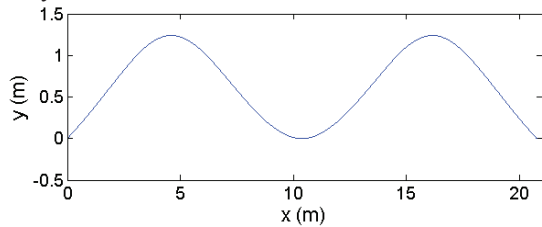

Figure 2: Etendue conserving curve for peak conditions [4]

For this study the number of x divisions N = 30; creating an x division dx = 0.6928m. Within the single target sections, the mirrors are simply created by dividing sections of the curve that lie within the bounds of dx, then aligning the mirrors so that they are accurately targeting the receiver. For the multiple target section, radiation splitters are used (see Figure 3) so that each section dx, contains two mirrors that target the different receivers.
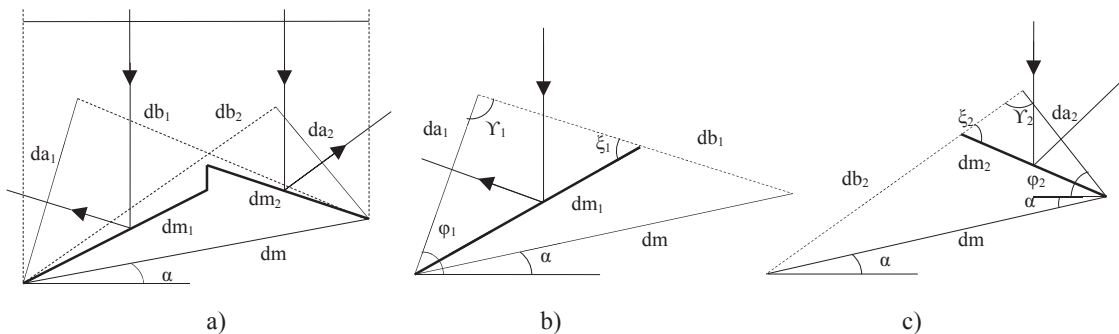

Figure 3: a) Radiation splitters and main mirror b) Discretized radiation splitter 1 c) Discretized radiation splitter 2 [2]

The equation sets describing the distance and angular quantities related to the two receivers (refer to Figure 3) are given as follows:

$$da_1 = dx\cos\phi_1 \tag{1}$$

$$db_1 = \sqrt{da_1^2 + dm^2 - 2da_1dm\cos(\phi_1 - \alpha)} \tag{2}$$

$$\frac{\sin\gamma_1}{dm} = \frac{\sin(\phi_1 - \alpha)}{db_1} \tag{3}$$

$$\gamma_1 = \arcsin\left(\frac{dm\sin(\phi_1 - \alpha)}{db_2}\right) \tag{4}$$

$$\xi_1 = 180° - \frac{\phi_1}{2} - \gamma_1 \tag{5}$$

$$dm_1 = \frac{da_1\sin\gamma_1}{\sin\xi_1} \tag{6}$$

$$da_2 = dx\cos\varphi_2 \tag{7}$$

$$db_2 = \sqrt{da_2^2 + dm^2 - 2da_2dm\cos(\phi_2 - \alpha)} \tag{8}$$

$$\frac{\sin\gamma_2}{dm} = \frac{\sin(\phi_2 + \alpha)}{db_2} \tag{9}$$

$$\gamma_2 = \arcsin\left(\frac{dm\sin(\phi_2 + \alpha)}{db_2}\right) \tag{10}$$

$$\xi_2 = 180° - \frac{\phi_2}{2} - \gamma_2 \tag{11}$$

$$dm_2 = \frac{da_2\sin\gamma_2}{\sin\xi_2} \tag{12}$$

The discretized curve is established up to the center point of the field, at which point it is reflected about the point to complete the discretized field. The field is therefore positioned and sized based on the peak scenario as that is the time of day in which maximum radiation can be harnessed. The angle of the mirrors is such that the normal bisects the angle through which light is reflected. For peak times of day this is simply represented as $\alpha = \dfrac{\phi}{2}$

The mirror field needs to move to track the sun throughout the day. The simplest model fixes an axis of rotation at the center of the mirror in x and y. The new mirror angle is then calculated simply by combining the angle associated with the mirror position and the angle of the incoming radiation $\mu = \dfrac{2\alpha + \theta}{2}$

However, at higher angles blocking and shading become significant. Therefore a model of etendue matching curves for off peak times is used for the lower angles.
This model also runs an unconstrained optimization, taking into account the incoming radiation angle such that the objective function becomes $f(x) = \left|\left[\cos(\phi_1 - \alpha) + \cos(\phi_2 + \alpha)\right] - \cos(\alpha - \theta)\right|$

The initial parabola is calculated as before and the optimization is run for the full domain rather than the midpoint. The new minimum of the curve is then found and the curve is reflected about that point to represent the final etendue conservation curve for that angle. For larger angles, this method could not be used as the maximum of the curve is reached around the midpoint of the domain and therefore when the optimization is run for the entire domain the curve furthest from the incoming sun will be driven to a height equivalent to that of the receiver. This large increase in height is due to the central section blocking the farther parabola from the sun completely. Using etendue conservation for larger incident angles becomes unpractical and therefore only tracking is used beyond 40°. The resulting off-peak curves for a sun angle of 20° and 40° are given in Figure 4a) and b), respectively.
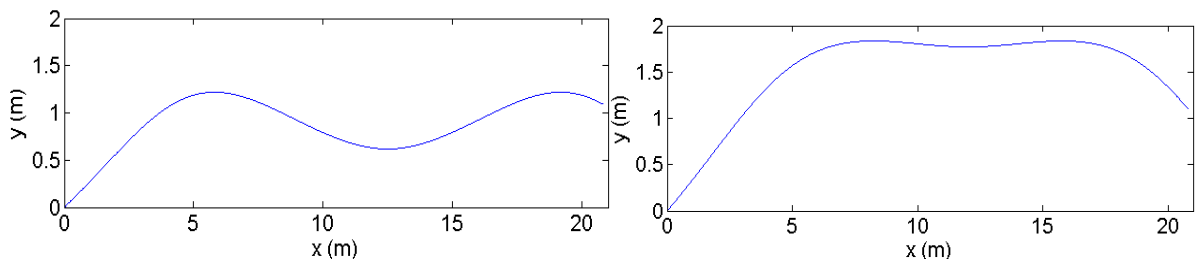

Figure 4: Off-peak mirror field for sun angles of a) 20°, and b) 40°

Once the off peak curve is obtained it is discretized and the mirrors are checked to ensure that they are targeting at the receiver accurately. The discretized mirrors are shown in Figure 5 for the two sun angles.

a)   b)
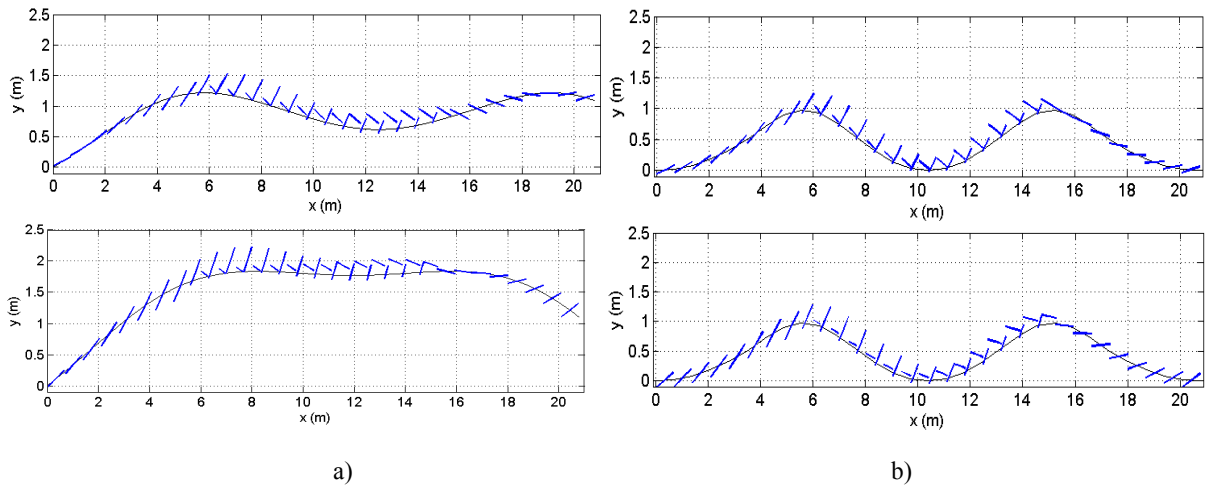
Figure 5: Sun angle 20° and 40° discretized mirror fields for a) etendue conserving off-peak curves, and b) mirrors tracking based on peak etendue-conserving curve

3. Two-dimensional CFD modeling

3.1 Computational domain and boundary conditions

The domain is modeled in *ANSYS Fluent v15.0* in both two and three dimensions. The advantage of using a CFD package rather than a ray tracing tool is that the CFD modeling provides an integrated environment for all simulations to be completed in. This is particularly important when transferring information for the radiation boundary condition from the two-dimensional model to the three-dimensional model.

The two-dimensional Computational Fluid Dynamics (CFD) model of the domain consists of both the mirror field and a trapezoidal receiver with four collector pipes of diameter 50mm (See Figure 6). The 2-D model functioned akin to a ray tracer, with discrete ordinates radiation modelling and fixed temperatures on all external boundaries. The entire model consists of solid regions that do not conduct heat but participate in radiation. This simulates the absorption and reflection in order to quantify the absorbed radiation flux on each collector pipe. The absorbed radiation flux profile is then used in a user-defined function that patches it in as a heat source for the three-dimensional model, thereby reducing the required computational domain for the conjugate three-dimensional CFD model, to be described next. The boundary conditions are listed in Table 1.

Table 1: Boundary conditions for 2-D CFD model.

Named selection	2-D Boundary condition
Radiation source	Specular radiation of 1000W/m^2 with a beam angle of 0.53$^{\mathbf{0}}$
Collector pipes	Fixed temperature $\varepsilon = 1$, T = 1.0K.
Receiver cavity walls	Fixed temperature $\varepsilon = 0$, T=1.0K
Transparent cover wall	Semi-transparent, coupled wall
Mirrors	Fixed temperature, specular reflection $\varepsilon = 0$, T= 1.0K
Mirror gaps and edges of domain	Fixed temperature $\varepsilon = 1$, T = 1.0K.

The two-dimensional model for peak conditions is modelled with a fine mesh, with 5.0mm edge mesh sizing on the mirrors, about 1.0mm on the collector pipes and 20.0mm cell sizing throughout the rest of the model. This resulted in a mesh with about 900 000 cells, the exact number depending on the detail of each mirror field. This

mesh size was obtained after a sensitivity study comparing total absorbed radiation by varying both mesh size and the angular discretization settings of the Discrete Ordinates radiation model. The latter includes the two solid angle increments and the pixilation using in *ANSYS* Fluent. Angular increments of 20 with 10 pixels each were found to be sufficient for comparison purposes. This meant that, in addition to the energy equation, a further $4 \times 20 \times 20 = 1600$ differential equations were solved in the discrete ordinates implementation of the Radiation Transport Equation, as each quadrant in two-dimensions is subdivided.
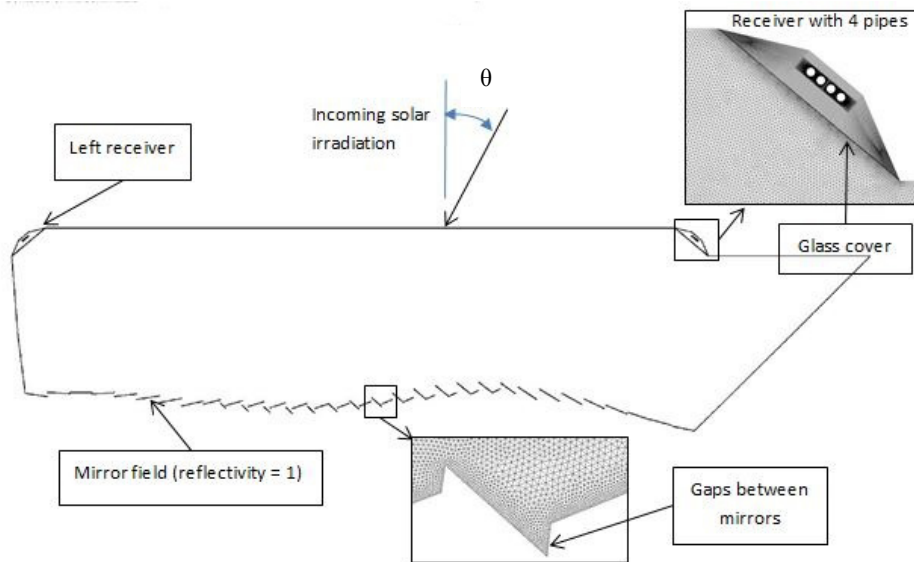

Figure 6: Two-dimensional CFD model domain and boundary conditions with inserted displaying mesh views (20° sun angle mirror field)
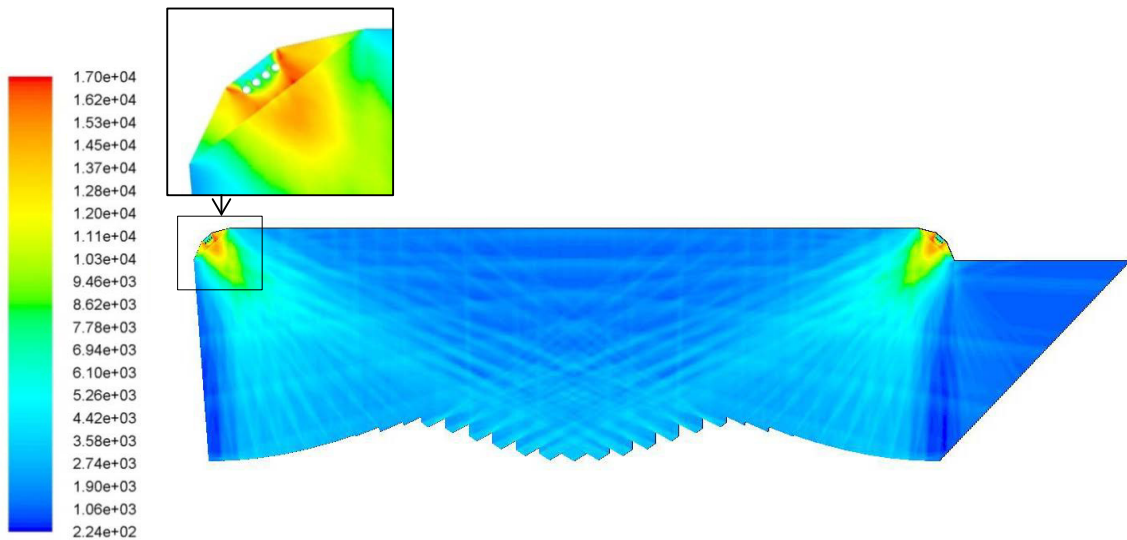
3.2 Results for two-dimensional radiation modeling

Figure 7. Incident radiation contours [W/m^2] for peak sun angle $\theta = 0^\mathbf{o}$, using Discrete Ordinates model

The incident radiation for the peak sun angle of 0° is shown in Figure 7 (above). The capturing of the targeting of the incoming Direct Normal Irradiation towards the two receivers can clearly be seen. The insert shows how the four absorber pipes absorb the concentrated radiation while the cavity walls reflect it. The effect of the different refractive index of the transparent glass cover is evident in the discontinuity of the radiation contours.

As the etendue conserving mirror layout seeks to improve the optical efficiency of the mirror field, a flat Compact Linear Fresnel model with 30 mirrors is used as the basis for comparison for both the sun tracking etendue curve with peak sizing and the off-peak etendue conserving mirrors. A series of simulations were run and are summarized in the total absorbed radiation [W] on all eight absorber pipes in Figure 8a) for a variation in sun angle. The etendue conserving mirror fields can be seen to display a significant advantage over a flat mirror field (shown in Figure 8c)).
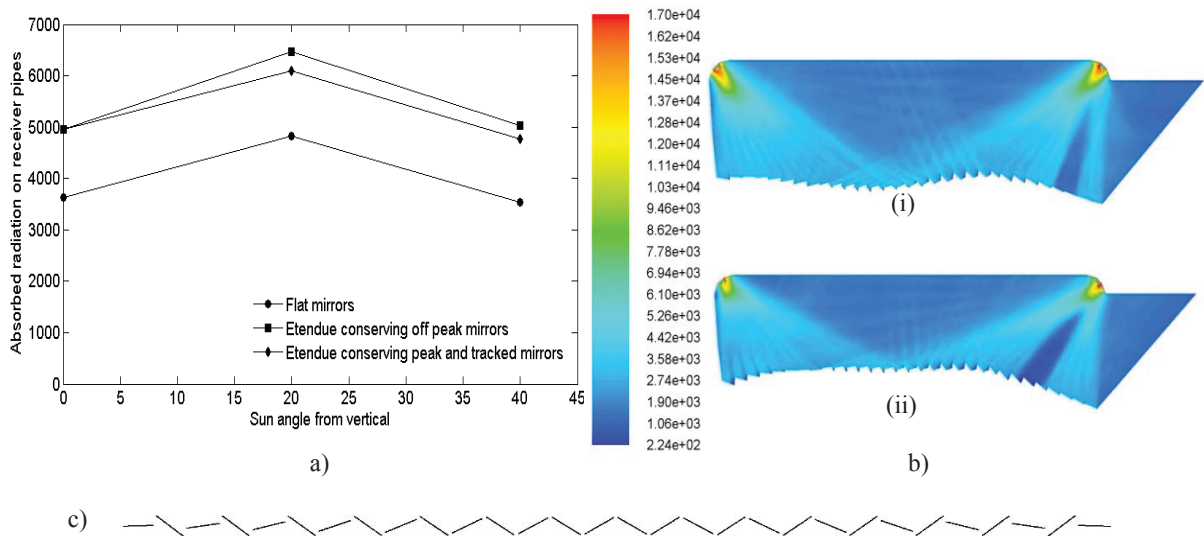

Figure 8. a) Graph of absorbed radiation versus sun angle for flat mirrors, peak etendue conserving and tracking mirrors and off peak etendue conserving mirror; b) Incident radiation contours [W/m^2] for off peak etendue conserving mirror fields at sun angles of (i) 20° and (ii) 40°; c) Flat 30-mirror field for 0° sun angle

The incident radiation contour for the two etendue conserving off-peak curves at 20° and 40° are shown in Figure 8b), with the shadow of the right receiver clearly visible.

For all the mirror fields included on the graph in Figure 8a) the absorbed radiation on the receiver pipes is higher for a sun angle of 20° than it is for the peak angle 0°. This is due partly to the fact that both receiver shadows fall on the mirror field during peak time, as opposed to the shadow of only the right receiver falling on the mirror field at higher sun angles. Moreover, there are fewer missed rays at and less blocking at higher incidence angles [5, 6].

The etendue conserving off-peak field has a higher total absorbed radiation on the receiver pipes but also maintains the symmetry of absorbed radiation between the two receivers, as shown in Table 2. This balance between the absorbed heat fluxes on the receivers is advantageous as it simplifies plant operation by creating uniform temperatures for other components in the power cycle.

Table 2: Absorbed radiation on left and right receivers for different mirror fields

Sun angle (^{0})	Absorbed radiation of receiver pipe [W]					
	Flat mirror field		Etendue conserving field		Etendue peak and tracking	
	Left	Right	Left	Right	Left	Right
0	1818	1819	2473	2474	2473	2474
20	2395	2436	3201	3269	3009	3088
40	1426	2117	2463	2573	2163	2598

4. Three-dimensional CFD modeling

4.1. Computational domain and boundary conditions

The 3-D computational domain is shown in Figure 9. The right receiver with its four pipes was modeled by extending the model through a depth of 1m. As a first approximation, the air in the cavity was treated as a solid with air properties (thermal conductivity of 0.03W/m-K), i.e., no natural convection was modeled. The sides of the computational domain were treated as symmetry boundaries with the insulation outer surfaces convecting with a surface heat transfer coefficient of 5W/m²-K to 300K, and radiating with an emissivity of 0.75 to a sky temperature of 271K and a mirror temperature of 305K, respectively. The thermal re-radiation is solved using the Discrete Ordinates model in *ANSYS* Fluent with a dual-band treatment. The glass cover material (with a thermal conductivity of 1.5W/m-K and a refractive index of 1.5) was given a selective absorption coefficient of 106 and 2300 W/m in the two wavelength bands: (0-4.25μm) and (4.25μm-1mm), respectively. This means that the emitted re-radiation from the absorber pipe and cavity walls would be absorbed by the glass depending on its temperature-dependent wavelength to mimic the greenhouse effect. The absorber pipes were given band-selective emissivity values of 0.95 and 0.1 while the cavity walls were set to emit/absorb 10% (based on Kirchhoff's law). The insulation thermal conductivity was set at 0.03W/m-K while that of the steel pipes were set at 54W/m-K.
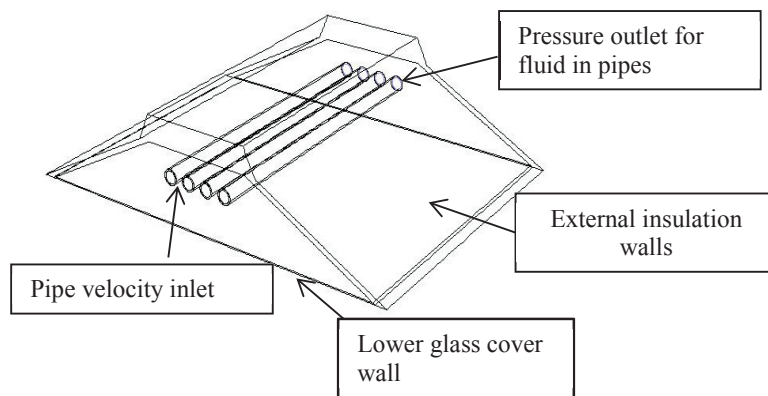

Figure 9. Three-dimensional model geometry and boundary condition locations

The solar load radiation heat flux [W/m²] source for each absorber pipe as obtained from the 2-D CFD simulation is displayed in Figure 10a). This flux was converted to a volumetric heat source for each pipe and applied to each pipe solid zone in the 3-D *ANSYS* Fluent model. The process involved interpolating each heat source data set to a temporary user-defined scalar that was then assigned to a user-defined memory location. From here it was assigned to a volumetric source during the calculation using a DEFINE user-defined function. The resulting volumetric heat source field is shown in Figure 10b).
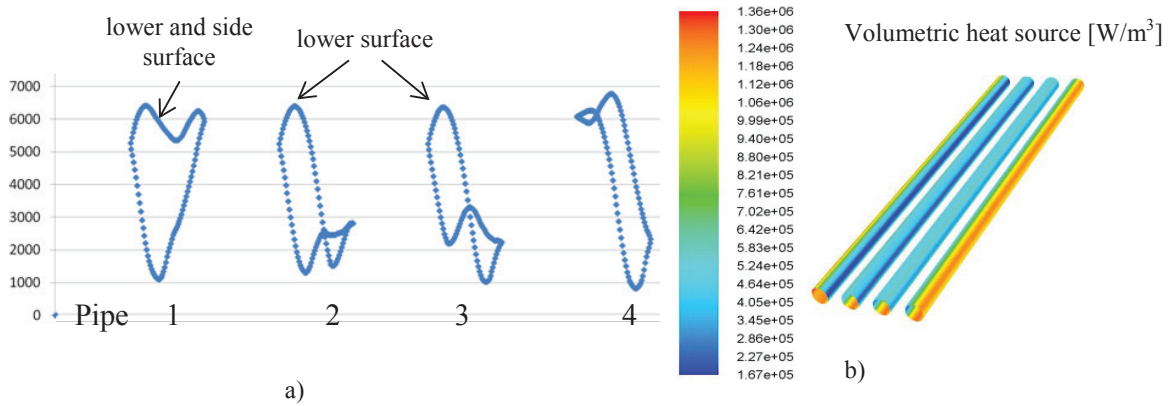
Figure 10. a) Heat flux [W/m^2] and b) 3-D volumetric heat source values [W/m^3] as obtained from 2-D CFD simulation for right receiver pipes

4.2 Results for three-dimensional heat transfer modelling

The steady-state simulated temperature field on the absorber pipe outer surface is depicted next to those of the receiver cavity walls in Figure 11 for a representative case. Water was used as heat transfer fluid flowing at an average inlet velocity of 0.1m/s, resulting in a heat transfer fluid temperature increase of about 1.2K per 1m length. This velocity corresponds to a Reynolds number of about 4000. The asymmetric heat transfer from the pipe material causes an asymmetric temperature profile on the pipe inside walls.
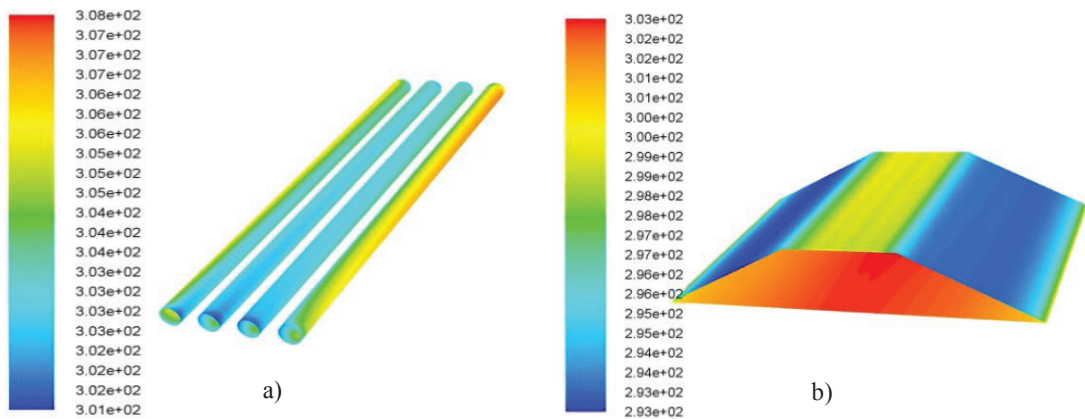

Figure 11. Temperature contours [K] on a) inside of absorber pipes and on b) inner surface of insulation and on glass cover

5. Conclusion and recommendations

A system where etendue is conserved represents a zero loss system; therefore designing a system that seeks to conserve etendue is equivalent to designing a system to minimize optical losses. The etendue conserving mirror field represented significant increases in the absorbed radiation flux on the receiver tubes, both for the tracking and the etendue conserving off-peak fields, but does not increase manufacturing requirements of the mirrors themselves as all mirrors are flat or slightly curved. However, the requirement that each mirror rotate and move up and down does increase the complexity of the mechanics required to realize the mirror field model and would likely require an

increase in the cost associated with the field. There is therefore a necessary tradeoff between optical efficiency and the cost associated with the system

In addition to an increase in the absorbed radiation of the receiver pipes, the symmetry obtained in the etendue conserving off-peak model represents an opportunity to simplify other processes within the plant. Linear Fresnel technology is therefore a cost-effective tenant of concentrated solar power and by creating a mirror field that significantly decreases the associated optical losses the technology becomes a more competitive alternative to parabolic trough technology.

It should be noted that the absorbed radiation flux on the receiver pipes in this study is dependent on the internal geometry of the receiver itself and therefore the efficiency of the system could also be improved by optimizing the receiver geometry. Apart from choosing the materials and geometry in the receiver with efficiency in mind, the reflective inner surfaces could be curved to create a secondary concentrator within the receiver, further increasing the absorbed radiation flux.

Acknowledgements

References

[1] Walker G, Von Backström TW, Gauché P. A Method of Increasing Collector Aperture in Linear Fresnel Solar Concentrators at High Zenith Angles. Proceedings of the 1st annual Southern African Solar Energy Conference; 2012 May 21-23; Stellenbosch, South Africa; 2012.

[2] Chaves J, Collares-Pereira M. Primary concentrator with adjusted etendue combined with secondaries associated to multiple receivers and with convection reduction. International patent WO2009142524 A1, 2009 Nov 26

[3] Mills DR, Morrison GL. Compact Linear Fresnel Reflector Solar Thermal Powerplants. *Solar Energy*.2000;68(3):263-283

[4] Chaves J, Collares-Pereira M. Etendue-matched two-stage concentrator with multiple receivers. *Solar Energy*.2010; 84:196-207

[5] Pye JD. System Modeling of the Compact Linear Fresnel Reflector [PhD Thesis]. Australia: University of New South Wales, 2008

[6] Häberle A, Zahler C, Lerchenmüller H, Mertins M, Wittwer C, Trieb F, Dersch J. The Solarmundo line focusing Fresnel collector. Optical and thermal performance and cost calculations. Presented at the 11th annual International SolarPACES Symposium, 2002 Sept 4-6, Zurich, Germany